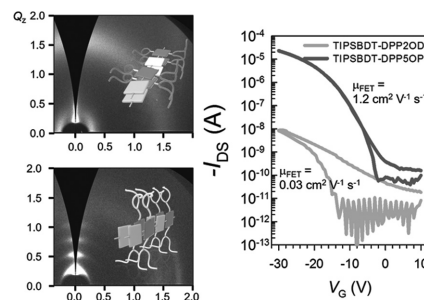


Coplanar Donor–Acceptor Semiconducting Copolymers to Achieve Better Conjugated Structures: Side-Chain Engineering

Mingyuan Pei, Ji-Hoon Kim, Sungmin On, Han-Koo Lee, Kilwon Cho,*
Do-Hoon Hwang,* Hoichang Yang*

It is reported on the allocation effects of branched alkyl chains, when used as solubility and ordering enhancers of the conjugated donor–acceptor (*D–A*) copolymer backbones, on the ordering and π – π overlapping of the copolymers, that drastically affect the electrical properties of organic field-effect transistors (OFETs). Triisopropylsilylethynyl-benzo[1,2-*b*:4,5-*b'*]dithiophene (TIPSBDT) and diketopyrrolopyrrole (DPP)-based copolymers, which have two linear alkyl spacers (methylene (*C1*) or butylene (*C4*)) between the DPP and side-substituent ($C_{10}H_{21}$) $CH(C_8H_{17})-$, are synthesized by Suzuki cross-coupling. These copolymer films are spun cast onto a polymer-treated SiO_2 dielectric surface, and some are further thermally annealed. The longer spacer, *C4*, is found to efficiently enhance the coplanarity and conjugation of the *D–A* backbone, while the *C1* does not. The resulting *C4*-bridged TIPSBDT-DPP-based copolymer readily develops a superior π -extended layer on the dielectric surface; the edge-on chains with randomly oriented side chains can be closely packed with a short π -planar distance ($d_{(010)}$) of 3.57 Å. Its properties are superior to those of the short spacer *C1* system with $d_{(010)} \approx 3.93$ Å. The *C4*-bridged TIPSBDT-DPP copolymer films yield a field-effect mobility up to $1.2 \text{ cm}^2 \text{ V}^{-1} \text{ s}^{-1}$ in OFETs, 12 times as higher than that of the *C1* spacer system.



1. Introduction

Organic field-effect transistors (OFETs) have attracted considerable research and industry attention because of their potential wearable device applications as low-cost, flexible, stretchable, and lightweight electronic components in wearable device displays, radio-frequency identification tags, and sensors.^[1,2] To achieve high electrical performance OFETs without any dopants, it is important to control the intra- and intermolecular ordering of the conjugated organic materials that serve as charge-carrier transport paths.^[3–5] Unlike small molecules which can self-assemble into highly ordered domains,^[6] conjugated polymers with high molecular-weight (M_w) tend to form a twisted or entangled chain conformation in solutions, preventing close π – π overlapping between these chains in solid states.^[5] However, conjugated polymers possess

M. Pei, S. On, Prof. H. Yang
Department of Applied Organic Materials Engineering
Inha University
Incheon 22212, South Korea
E-mail: hcyang@inha.ac.kr
Dr. J.-H. Kim, Prof. D.-H. Hwang
Department of Chemistry
Chemistry Institute for Functional Materials
Pusan National University
Busan 46241, South Korea
E-mail: dohoonhwang@pusan.ac.kr
Dr. H.-K. Lee
Pohang Accelerator Laboratory
Pohang 37673, South Korea
Prof. K. Cho
Department of Chemical Engineering
POSTECH, Pohang 37673, South Korea
E-mail: kwcho@postech.ac.kr

excellent deformability and high-temperature stability (greater than 250 °C), which make them more useful as active channel materials in flexible electronics compared to less-deformable small molecules.^[2]

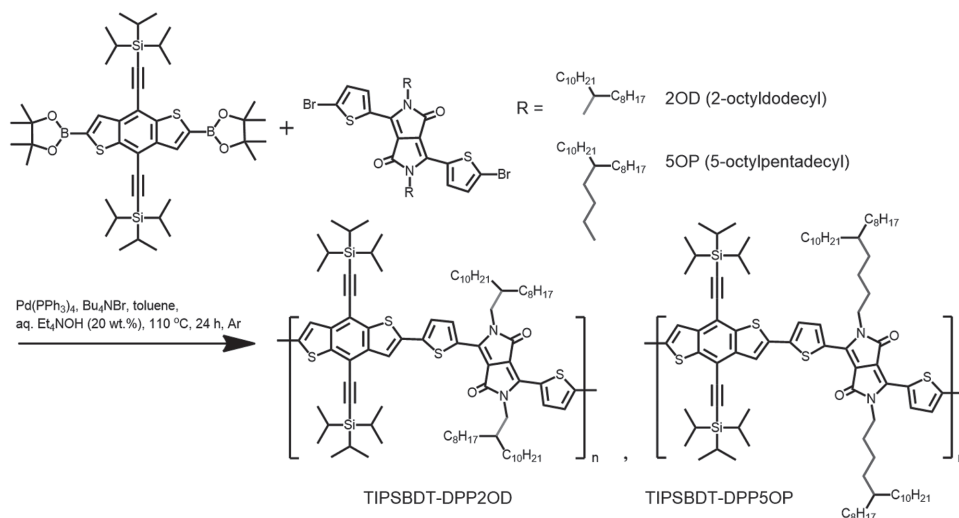
One powerful strategy to improve the intra- and intermolecular interactions between semiconducting polymers is the design of conjugated backbones to include alternated electron donor–acceptor (*D–A*) building blocks. Specifically, the push–pull structure of alternated planar *D* and *A* units leads to a polymer backbone with a less opportunity for torsional twist between conjugated segments, yielding less energetic backbones.^[3,7,8] The better coplanarity and smaller reorganization energies of the *D–A* copolymers can induce more compact π – π overlapping paths in cast films. Diketopyrrolo[3,4-*c*]pyrrole (DPP) derivatives have emerged as promising *A* blocks to design low band gap copolymers for OFET and organic photovoltaics (OPV) applications.^[9] Combined with DPP derivatives, triisopropylsilylethynyl-benzo[1,2-*b*:4,5-*b'*]dithiophene (TIPSBDT) as an electron-rich *D* block has been used to synthesize *D–A* copolymers due to its rigid and extended π -conjugation.^[7] It is known that long alkyl side chains introduced to rigid and planar *D–A* backbone segments improve the solubility of copolymers.^[10–12] However, the bulky and flexible chains weaken the interchain attractions, which govern charge-carrier transport in the *D–A* copolymer.^[13–18]

Recently, Kim et al. reported that a TIPSBDT and DPP-based copolymer, poly[4,8-bis(triisopropylsilyl-ethynyl)-benzo[1,2-*b*:4,5-*b'*]dithiophene-alt-3,6-bis-(thiophen-2-yl)-*N,N'*-bis(2-octyl-1-dodecyl)-1,4-dioxo-pyrrolo[3,4-*c*]pyrrole] (TIPSBDT-DPP2OD) (Scheme 1) with an HOMO (highest occupied molecular orbital) energy level below –5.50 eV could produce a power conversion efficiency as high as 8.0% and high open-circuit voltages greater than 0.9 V in OPVs

when blended with PC₇₁BM, originating from the electron-withdrawing carbon–carbon triple bond in the bulky and highly soluble TIPS side moieties.^[7] In addition, the polymer-based OFETs showed field-effect mobility (μ_{FET}) values up to 0.12 cm² V^{–1} s^{–1}. However, we found that the branched chain, (C₁₀H₂₁)CH(C₈H₁₇)–, which was introduced to each DPP segment with the very short methylene spacer, –CH₂– (referred to as C1), considerably degraded the intra- and intermolecular ordering in both solutions and films. Particularly, it was hard to extend the ordered domains in cast films, originating from the steric hindrance of the bulky branched alkyl chains closely attached to the DPP segments.

Meager et al. reported that the spacer length between DPP and branched alkyl substituents significantly affected the orientation of thieno[3,2-*b*]thiophene-DPP-based copolymers; a drastic improvement was observed in OPV and OFET performance upon moving the alkyl branching point further from the backbone.^[14] Kim and co-workers also reported that the side-chain tuning for DPP-based copolymers with selenophene-vinylene-selenophene could significantly affect molecular ordering and intermolecular π -overlap distance.^[19,20] They reported that the highest hole mobility obtained was with the introduction of a linear hexylene spacer between a branched alkyl chain and DPP segment.

Here, we investigated how the allocation of branched alkyl chains from the conjugated *D–A* backbone influence the intra- and intermolecular conformations of the corresponding semiconducting copolymers, which govern the solution processability and electrical properties of organic electronics. Two TIPSBDT-DPP-based copolymers, TIPSBDT-DPP2OD and poly[4,8-bis(triisopropylsilylethynyl)-benzo[1,2-*b*:4,5-*b'*]dithiophene-alt-3,6-bis-(thiophen-2-yl)-*N,N'*-bis(5-octylpentadecyl)-1,4-dioxo-pyrrolo[3,4-*c*]pyrrole] (TIPSBDT-DPP5OP), with the different alkyl



■ Scheme 1. Chemical structures and synthesis of the TIPSBDT-DPP2OD and TIPSBDT-DPP5OP copolymers used in this study.

spacers (C1 and butylene (referred to as C4)) between the DPP and (C₁₀H₂₁)CH(C₈H₁₇)– chains, were synthesized by Suzuki cross-coupling (Scheme 1). The longer spacer, C4, drastically enhanced the coplanarity and conjugation of the TIPSBDT-DPP5OP copolymer, which had an M_w of 26 760 g mol⁻¹ (smaller than the 35 790 g mol⁻¹ of the TIPSBDT-DPP2OD copolymer). These D–A copolymer films were spun cast onto a polymer-treated silicon dioxide (SiO₂) dielectric surface from chlorobenzene (CB) solutions, and some were further annealed at 200–300 °C. By inserting the longer spacer between DPP and (C₁₀H₂₁)CH(C₈H₁₇)–, the resulting TIPSBDT-DPP5OP copolymer could be tuned to form highly ordered and π -overlap extended domains of edge-on chains on the dielectric surface, with a narrow π - π overlap spacing ($d_{(010)}$) up to 3.57 Å, in comparison to the less-conjugated short spacer system with a wider $d_{(010)}$ of 3.93 Å. Better ordering and shorter π - π overlapping provided TIPSBDT-DPP5OP OFETs with the benefit of a μ_{FET} value greater than 1.2 cm² V⁻¹ s⁻¹, 12 times higher than that of the TIPSBDT-DPP2OD system. Proper side chains to minimize steric hindrance provide new insight into the molecular design of high-performance D–A copolymer-based semiconductors.

2. Results and Discussion

2.1. Material Characteristics

General characteristics of TIPSBDT-DPP-based copolymers synthesized by Suzuki cross-coupling (Scheme 1) are summarized in Table 1. Note that all copolymers used in this study were extracted from the synthesized powders by soxhlet extraction with chloroform (CF). The chemical structures of the TIPSBDT-DPP-based copolymers were identified by ¹H-nuclear magnetic resonance (NMR) (Figures S1 and S2, Supporting Information). The number average molecular weight (M_n) values of the TIPSBDT-DPP2OD and TIPSBDT-DPP5OP copolymers were 35 790, and 26 760 g mol⁻¹, respectively, and the polydispersity index (PDI) values of the copolymers were 2.30 and 2.96, as determined by gel permeation chromatography (GPC) analysis (Figure S3,

Supporting Information). The relatively low- M_n of TIPSBDT-DPP5OP copolymer was mainly related to the decreased solubility driven by its enhanced coplanar structure.

Figure 1a represents the ultraviolet-visible (UV-vis) absorption spectra of the copolymers in CB solutions and spun cast films. Detailed optoelectrical properties, such as absorption maxima (λ_{max}), edge (λ_{edge}), and optical band gap (E_g^{opt}), are listed in Table 1. The TIPSBDT-DPP2OD copolymer in both the solution and film clearly exhibited 0–0 and 0–1 absorption peaks at 770 and 690 nm, respectively. In contrast, the TIPSBDT-DPP5OP copolymer showed broad UV-vis absorption spectra ranging from 500 to 1000 nm, with a peak at 760 nm. The different absorption characteristics of these polymers yielded discernible colors in the corresponding solutions (Figure S4, Supporting Information). The broad UV-vis absorption of the TIPSBDT-DPP5OP copolymer was mainly related to the enhanced coplanarity driven by the relatively long spacer, C4, instead of C1. The branched side chain (C₁₀H₂₁)CH(C₈H₁₇)– connected to the long spacer was expected to effectively improve π -conjugated structure of the TIPSBDT-DPP backbones compared to the methylene spacer, C1.

The HOMO and lowest unoccupied molecular orbital (LUMO) energy levels of these copolymers were calculated from the oxidation cyclic voltammetry (CV) profiles (Figure 1b). The HOMO (and LUMO) energies of TIPSBDT-DPP2OD and TIPSBDT-DPP5OP copolymers were calculated as –5.44 (–4.00) eV and –5.28 (–4.04) eV, respectively. As expected, the optical band gap value of TIPSBDT-DPP5OP, 1.24 eV, was much narrower than that (1.44 eV) of the TIPSBDT-DPP2OD system. Additionally, the electrochemical band gap (based on reduction CV profiles, Figure S5, Supporting Information) of TIPSBDT-DPP5OP is 0.2 eV lower than that of TIPSBDT-DPP2OD (1.77 eV), which matches well with the difference in optical band gaps. Thermogravimetric analysis (TGA) profiles of the powder-like copolymers showed ≈5% weight losses at 400 and 412 °C (Figure S6a, Supporting Information). In addition, differential scanning calorimetry (DSC) analysis measured thermal properties of the copolymers; a melting temperature (T_m) at 217 °C was indicated for TIPSBDT-DPP2OD copolymer, but TIPSBDT-DPP5OP one

Table 1. Thermal, optical, and electrochemical properties of TIPSBDT-DPP2OD and TIPSBDT-DPP5OP copolymers.

| Copolymer | $M_n^a)$ [g mol ⁻¹] | PDI | $T_d^b)$ [°C] | λ_{max} [nm] | | $E_g^{\text{optd)}$ | $E_g^{\text{elece)}$ | HOMO ^{f)} | LUMO ^{g)} | LUMO ^{h)} |
|----------------|------------------------------------|------|------------------|-----------------------------|--------------------|---------------------|----------------------|--------------------|--------------------|--------------------|
| | | | | Solution or film | Film ^{c)} | | | | | |
| TIPSBDT-DPP2OD | 35 790 | 2.30 | 400 | 690, 770 | 861 | 1.44 | 1.77 | –5.44 | –4.00 | –3.67 |
| TIPSBDT-DPP5OP | 26 760 | 2.96 | 412 | 760 | 1000 | 1.24 | 1.57 | –5.28 | –4.04 | –3.71 |

^{a)} M_n and PDI of the polymers were determined by GPC calibrated with PS standards in CB; ^{b)}Temperature at 5% weight loss; ^{c)}Films were spun cast onto a quartz plate from CB solutions; ^{d)}Calculated from the absorption band edge of the copolymer films, $E_g^{\text{opt}} = 1240/\lambda_{\text{edge}}$; ^{e)}Calculated from the HOMO and LUMO were measured by CV of the copolymer films; ^{f)}HOMO = $-e(E_{\text{onset}}^{\text{ox}} + 4.64)$ (eV); ^{g)}LUMO = $E_g^{\text{opt}} + \text{HOMO}$ (eV); ^{h)}LUMO = $-e(E_{\text{onset}}^{\text{red}} + 4.64)$ (eV).

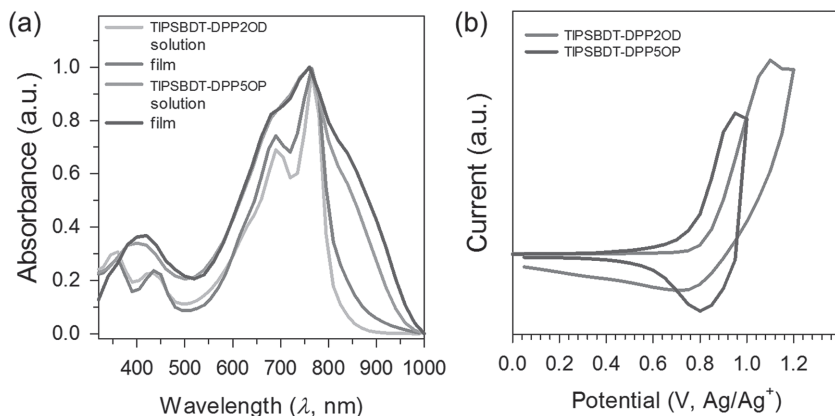


Figure 1. a) UV-vis spectra of TIPSBDT-DPP-based copolymers in solutions and spun-cast films. b) Oxidation CV curves of each thin film on an electrode in a 0.1 M tetrabutyl ammonium tetrafluoroborate (TBABF₄)-acetonitrile solution with a scan rate of 50 mV s⁻¹.

did not show any endothermic peaks within the temperature scanning range of 30–350 °C (Figure S6b, Supporting Information).

To estimate the coplanarity of the TIPSBDT-DPP-based copolymers with different spacers, such as C1 and C4, density functional theory calculations of the *D*–*A* dimers simplified for the semiconducting copolymers (Figure 2) were conducted using B3LYP functional and 6-31G(d) basis sets. The energy states of both the simplified dimers were well delocalized along the conjugated segments (Figure 2). Calculated dihedral angles for the *D*–*A* dimers, where A1 and A3 are dihedral angles between TIPSBDT unit and DPP unit for different inner molecular segments, and A2 is dihedral angle of the bond across the bridge between adjacent molecular segments. Different bridge units significantly affect the molecular architecture. The dihedral angles between the TIPSBDT and DPP units for TIPSBDT-DPP2OD are 8.06 and 13.01°, much larger than those for TIPSBDT-DPP5OP with values of 2.84 and 5.20°, respectively. Similarly, the dihedral angle of bridge between adjacent segments for TIPSBDT-DPP5OP (11.49°) is also smaller than TIPSBDT-DPP2OD (14.85°), indicating more enhanced coplanarity of the TIPSBDT and DPP5OP backbone units. This suggests that the introduction of the C4 spacer increases the coplanarity of the conjugated TIPSBDT-DPP *D*–*A* backbone segments due to an efficient decrease in steric hindrance by

the branched (C₁₀H₂₁)CH(C₈H₁₇)– chains. In addition, with the side chains varied from C1 spacer to C4 spacer, the shape of molecular chains changed more akin to straight line with decreasing of A2. In this case, the π -orbital overlap between neighboring segments is increased, leading to changes in the frontier orbital energy levels and decrease in band gaps, in accordance with band gap values mentioned above.

2.2. Allocation Effects of Branched Alkyl Chains from Conjugated Backbones

As channel layers in OFETs, 20–25 nm thick semiconducting films were spun cast onto polystyrene (PS)-grafted SiO₂ bilayer dielectrics (referred to as gPS-SiO₂) dielectrics from CB, and some were further annealed for 30 min at different annealing temperatures (*T*_A) values of 200 and 250 °C and for 10 min at 300 °C.

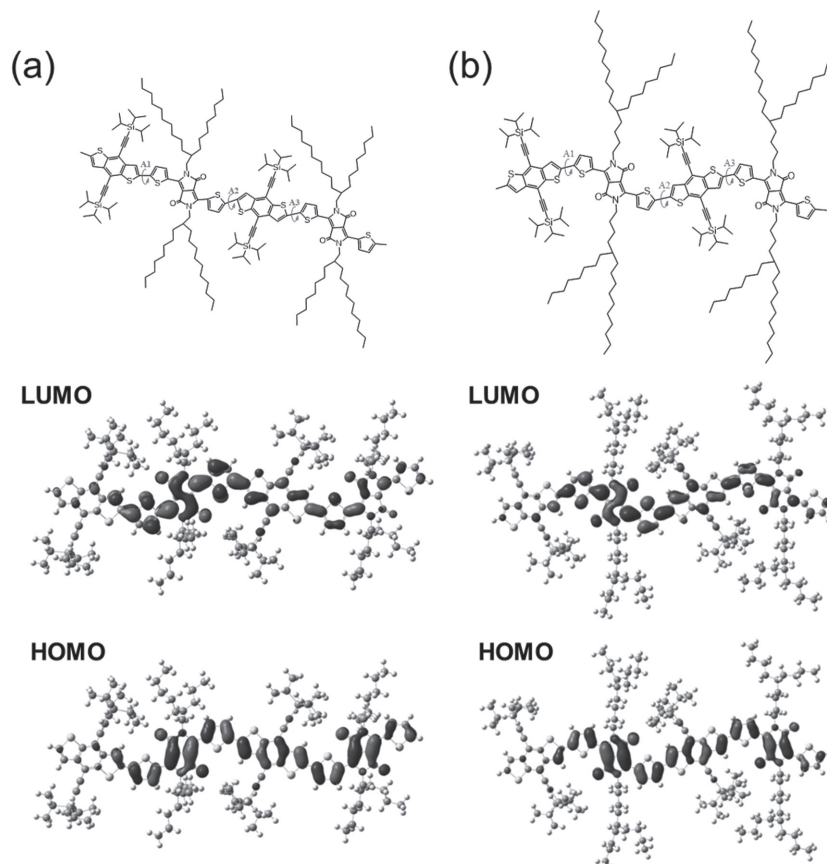


Figure 2. Schemes of HOMO and LUMO energy levels, energy-minimized molecular geometries of the resulting simplified a) TIPSBDT-DPP2OD (A₁ = 8.06°; A₂ = 14.85°; A₃ = 13.01°) and b) TIPSBDT-DPP5OP dimers (A₁ = 2.84°; A₂ = 11.49°; A₃ = 5.20°) showing different dihedral angles.

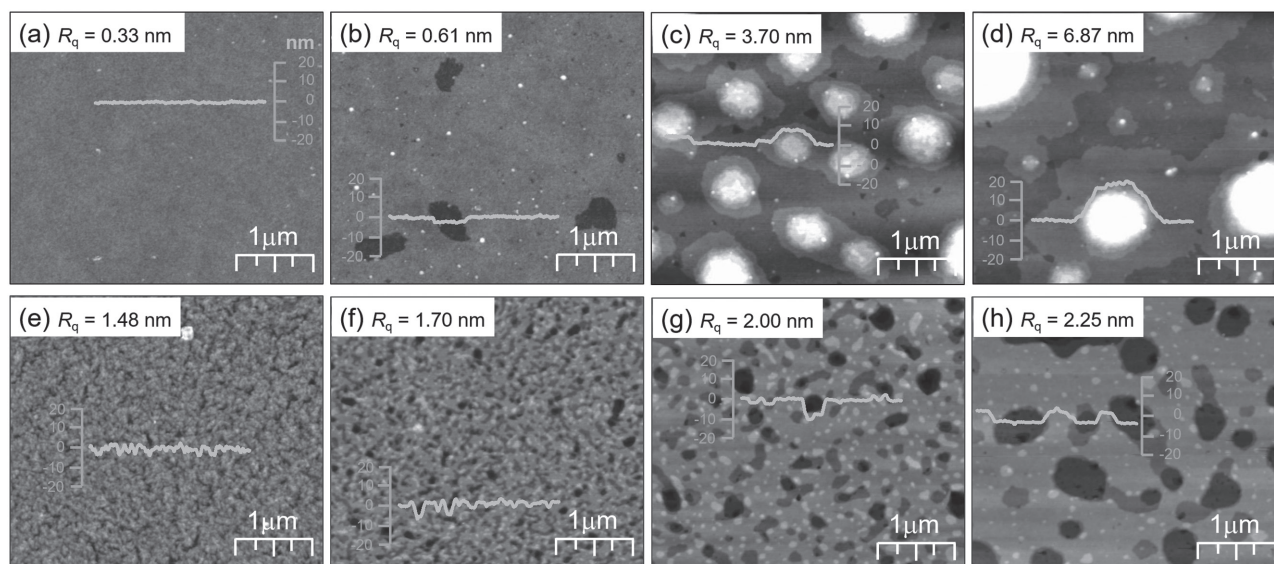


Figure 3. AFM topographies of a–d) TIPSBDT-DPP2OD and e–h) TIPSBDT-DPP5OP copolymer films on the *g*PS-treated SiO₂ surfaces before and after thermal annealing at various T_A for 30 min (or 10 min at 300 °C): a,e) as-spun, b,f) 200 °C, c,g) 250 °C, d,h) 300 °C (The insets represent the cross-sectional height profiles extracted from (a) to (h)).

Figure 3 shows typical atomic force microscopy (AFM) topographies of these spun-cast copolymer films before and after annealing. First, the AFM topography of the untreated TIPSBDT-DPP2OD copolymer film showed a featureless and very smooth layer (Figure 3a). After annealing at different T_A values, the resulting films showed layered structures with a molecular layer (ML)-stacked step height. As shown in Figure 3b–d, however, the annealed films were locally dewetted: specifically, after annealing at T_A greater than $T_m = 217$ °C. Additionally, the surface roughness (referred to as root-mean square roughness, R_q) drastically increased from 0.33 (for untreated) to 6.87 nm (for 300 °C) after thermal annealing at different T_A values. In particular, the lateral disconnection between π -overlapped structures in the 300 °C-annealed sample severely degraded the charge-carrier transport in OFETs (discussed later). In contrast, as-spun TIPSBDT-DPP5OP film showed small-sized domains and the annealed films contained continuous layer structures, with R_q values ranging from 1.48 to 2.25 nm depending on the variations in the surface coverage of each ML thick layer with increasing T_A (Figure 3f–h). As shown in

Figure 3h, specifically, the 300 °C-annealed film contained a long-range π -extended layer with a height variation of multiplied ML thickness of about 2.40 nm (discussed in 2D grazing-incidence X-ray diffraction (GIXD) results).

Moreover, the ordered structures in the TIPSBDT-DPP copolymer films were investigated using synchrotron-based GIXD analysis and the structural information is summarized in Table 2. As shown in Figure 4, the 2D GIXD patterns of these cast films clearly revealed the discernible chain ordering and π -conjugated orientations, originating from the different steric hindrance between 2OD and 5OP side chains. The bulky (C₁₀H₂₁)CH(C₈H₁₇)– chains closely attached to DPP segments prevented the close π – π overlapping between the TIPSBDT-DPP2OD copolymer chains, yielding the less-crystalline as-cast film, where most of the chains had a “face-on” conformation, i.e., the conjugated (010) planes were parallel to the polymer-treated SiO₂ surface (Figure 4a). After annealing, however, the resulting films showed intense X-ray reflections of (*h*00) crystal planes along the Q_z axis in both the 2D GIXD patterns and 1D out-of-plane X-ray profiles (Figure S7, Supporting Information). The results strongly support that the

Table 2. Structural information of the ordered chains in TIPSBDT-DPP-based copolymer films.

| Films | TIPSBDT-DPP2OD | | | TIPSBDT-DPP5OP | | |
|---------|-----------------|----------|-----------------|-----------------|----------|-----------------|
| | $d_{(100)}$ [Å] | FWHM [°] | $d_{(010)}$ [Å] | $d_{(100)}$ [Å] | FWHM [°] | $d_{(010)}$ [Å] |
| As-spun | – | – | – | 22.4 | 16.5 | 3.57 |
| 200 °C | 20.3 | 4.1 | 3.93 | 23.3 | 8.9 | 3.57 |
| 250 °C | 19.6 | 7.6 | 3.93 | 23.3 | 5.1 | 3.57 |
| 300 °C | 19.6 | 7.6 | 3.93 | 23.3 | 3.8 | 3.59 |

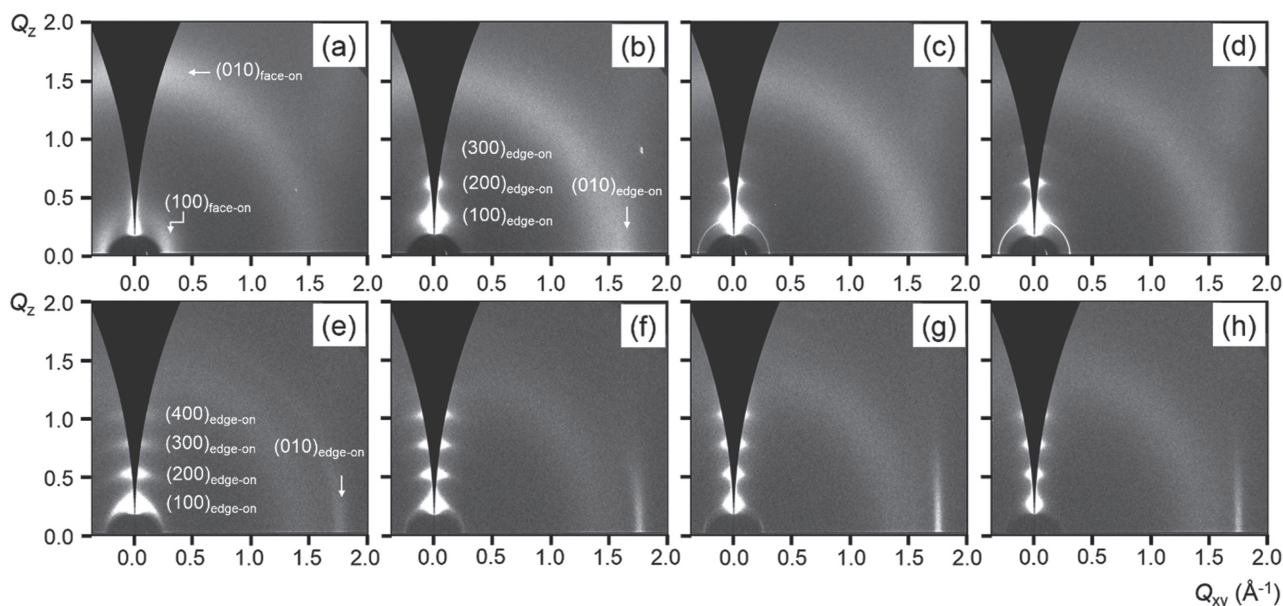


Figure 4. 2D GIXD patterns of a–d) TIPSBDT-DPP2OD and e–h) TIPSBDT-DPP5OP copolymer films on the *g*PS-treated SiO₂ surfaces before and after thermal annealing at various T_A for 30 min (10 min at 300 °C): a,e) as-spun, b,f) 200 °C, c,g) 250 °C, d,h) 300 °C.

annealed films contained “edge-on” chains, which were oriented perpendicular to the dielectric surface. Based on the periodic X-ray reflections of the (*h*00) planes along the Q_z axis (Figure S7a, Supporting Information), the distance between the conjugated backbones, $d_{(100)}$ ($=2\pi/\Delta Q_{(100)}$), which were separated by the side chains, was 20.3 Å (for 200 °C), and decreased slightly to 19.6 Å with an increase in T_A . However, the π - π overlap distance, $d_{(010)}$, remained at 3.93 Å, before and after thermal annealing.

In contrast, the 2D GIXD pattern of an as-spun TIPSBDT-DPP5OP film exhibited intense X-ray diffractions (Figure 4e), corresponding to the preferential orientation of the (*h*00) and (010) planes along the Q_z and Q_{xy} axes, respectively. The result supports that the copolymer chains could be readily crystallized and highly ordered with an “edge-on” conformation on the surface. In particular, based on the full width at half maximum (FWHM) in the azimuthal scan profiles extracted at $Q_{(100)} \approx 0.32 \text{ \AA}^{-1}$ (Table 2, Figure S8, Supporting Information), it was found that the crystallinities and the portions of “edge-on” chains in these TIPSBDT-DPP5OP films increased monotonically with increasing T_A (Figure 4f–h and Figure S7b, Supporting Information). In addition, the $d_{(100)}$ values increased from 22.4 to 23.3 Å with an increase in T_A , but the $d_{(010)}$ values were consistent at 3.57–3.59 Å, independent of T_A . Note that the π - π overlap distance between the ordered TIPSBDT-DPP5OP copolymers was much smaller than that of the TIPSBDT-DPP2OD system.

Typical π - π overlap distances of organic semiconductors have been reported as follows: 3.81–3.87 Å for poly(3-hexyl thiophene),^[5,21] $\approx 3.72 \text{ \AA}$ for poly[2,5-bis(3-tetradecylthiophen-2-yl)thieno[3,2-*b*]thiophene] (pBTTT-C14),^[22]

and 3.46–3.90 Å for DPP-based copolymers, which can yield high μ_{FET} values (greater than $1.0 \text{ cm}^2 \text{ V}^{-1} \text{ s}^{-1}$) in OFET (Table S1, Supporting Information).^[3,23–34] The electrical properties of these conjugated polymer-based OFETs tend to be enhanced with a decrease in the π - π overlap distance. It was expected that the relatively loose π - π stacking (3.93 Å) of the TIPSBDT-DPP2OD chains would degrade the charge-carrier transport along the stacked conducting paths in solid films.

To further investigate the in-plane orientations of the π -conjugated TIPSBDT-DPP backbone planes, synchrotron-based near-edge X-ray absorption of fine structure (NEXAFS) spectroscopy was conducted on the as-spun and 250 °C-annealed films in partial electron yield (PEY) detection mode.^[35] NEXAFS spectroscopy provides the information for the average orientation of the π -conjugated planes in organic semiconducting films by collecting carbon *K*-edge spectra obtained from various incidence angles (θ) of the p-polarized photon beam with respect to the plane of the film surface (the inset in Figure 5a).^[36,37] Based on the NEXAFS analysis for these TIPSBDT-DPP-based films, the average tilting angle (α) values of these conjugated planes with respect to a substrate were derived.^[36,38]

Figure 5 shows the typical NEXAFS spectra of the TIPSBDT-DPP copolymer films presenting the following signals: the π^* (C=C) orbital at 285.6 eV, the σ^* (C-S) orbital at 286.5 eV, the σ^* (C-H) orbital at 288.6 eV, the σ^* (C-C) orbital around 293.7 eV, and several σ^* orbitals (C=C) in the broad energies ranging from 298 to 310 eV. Based on the NEXAFS spectra, the variations in peak intensity (I_v) of the π^* orbitals were fitted according to previous literature.^[39] The θ -dependent intensities of the π^* orbitals are

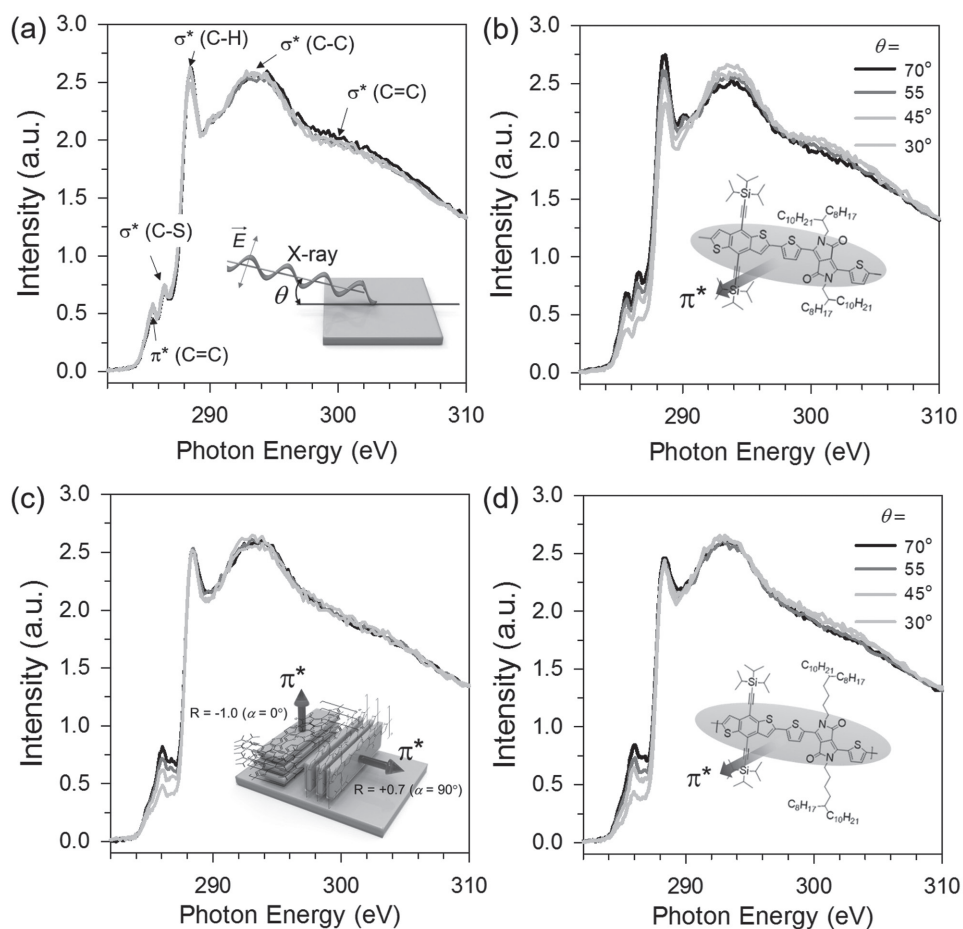


Figure 5. NEXAFS spectra of the TIPSBDT-DPP-based films a,c) before and b,d) after annealing at $T_A = 250\text{ }^\circ\text{C}$: a,b) TIPSBDT-DPP2OD and c,d) TIPSBDT-DPP5OP. The inset schemes represent a) the incident X-ray beam injected on a film with a given θ value and c) the variations in R depending on the average orientations of the π^* orbitals. Note that the R values can vary from +0.7 (parallel orientation of the π^* orbital; $\alpha = 90^\circ$), to 0 (random orientation; $\alpha = 54.7^\circ$ known as a magic angle), and -1 (perpendicular orientation; $\alpha = 0^\circ$).

usually expressed by the dichroic ratio, $R = [I(90^\circ) - I(0^\circ)] / [I(90^\circ) + I(0^\circ)]$, which defines the difference between the intensities at $\theta = 90^\circ$ and 0° , divided by their sum (the inset in Figure 5c).^[35] In addition, the θ -dependent intensities of the σ^* (C–C) orbital reflect the side-chain orientations, but they are difficult to quantify due to their less-ordered structures and partial backbone contributions.^[39]

The peak intensities of the π^* and σ^* orbitals in the NEXAFS spectrum of the as-spun TIPSBDT-DPP2OD film were independent of θ (Figure 5a). In contrast, those of the $250\text{ }^\circ\text{C}$ annealed films clearly showed a θ -dependent variation. The peak intensities of the π^* orbitals increased and the peak intensities of the σ^* orbitals decreased with an increase in θ , indicating the preferred orientation of conjugated planes rather than a random orientation. Unlike TIPSBDT-DPP2OD, the peak intensities of the π^* orbital in the NEXAFS spectra of both the untreated and TIPSBDT-DPP5OP films tended to increase with an increase in θ , while there was no θ -dependent intensity of the σ^* orbital.

From the $I_V \cdot \cos^2\theta$ profiles (Figure 6), the α_{π^*} (R) values of the overall conjugated backbone planes in the TIPSBDT-DPP2OD films were calculated to be 54.3° (0.012) in the as-spun film and 70.7° (0.473) in the $250\text{ }^\circ\text{C}$ -annealed film (Table 3). These values are consistent with the chain orientations inferred from the corresponding 2D GIXD results (Figure 4a–d, and Figure S7a, Supporting Information). In the TIPSBDT-DPP5OP, the α_{π^*} (R) values of the overall conjugated backbone planes in both the as-spun and $250\text{ }^\circ\text{C}$ annealed films were 68.9° (0.427) and 73.6° (0.517), respectively.

2.3. TIPSBDT-DPP Copolymer-Based OFETs

To characterize the electrical properties of the TIPSBDT-DPP-based copolymers as active channel materials of OFETs, top-contact Au S/D electrodes were patterned on the as-spun and thermally annealed films to fabricate OFETs (the inset in Figure 7b). Figure 7 shows typical drain current–gate voltage (I_D – V_G) transfer curves and the corresponding

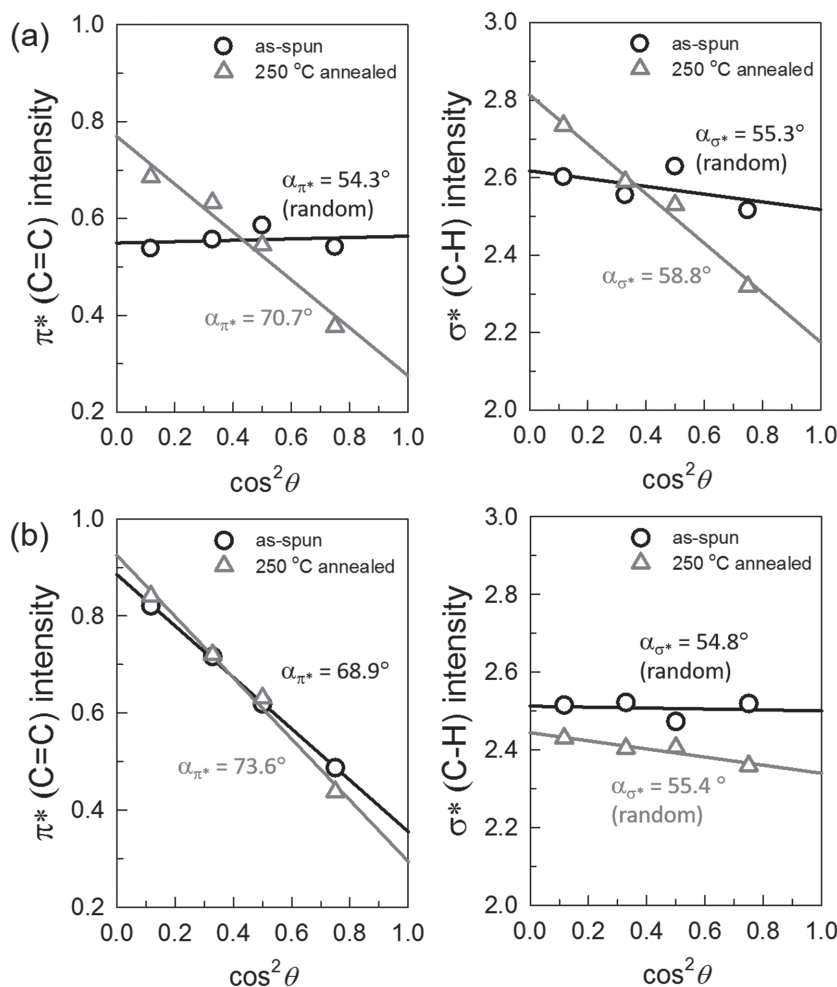


Figure 6. The intensity variations in π^* and σ^* orbitals extracted from the NEXAFS spectra: a) TIPSBDT-DPP2OD and b) TIPSBDT-DPP5OP.

$I_D^{0.5}$ - V_G curves of TIPSBDT-DPP copolymer-based OFETs operated in the saturation regime (at drain voltage, $V_D = -30$ V) and the T_A -dependent μ_{FET} variations. I_D - V_D output curves of all the samples present typical *p*-type transistor behaviors (Figure S9, Supporting Information). Electrical properties of the resulting OFETs are summarized in Table 4. Among TIPSBDT-DPP2OD-based OFETs, first, the 200 °C-annealed film yielded the best electrical properties

an easier path for hopping the carriers along neighboring conjugated chains, due to stronger π -stacking interactions.^[35] The branched alkyl chains connected by the longer alkyl spacer to the *D*-*A* backbones yield better intra- and intermolecular π - π overlapping. This characteristic is beneficial for the construction of ordered π - π stacking structure.

3. Conclusions

The location of a branched alkyl point on the coplanar *D*-*A* backbone was changed to tune the intra- and intermolecular conformations of the copolymers, which govern their solution processability and electrical properties in organic electronics. The TIPSBDT-DPP-based copolymers TIPSBDT-DPP2OD and

in OFET; $\mu_{\text{FET}} = 0.10 \text{ cm}^2 \text{ V}^{-1} \text{ s}^{-1}$ and on/off current ratio ($I_{\text{on}}/I_{\text{off}}$) $> 10^5$ compared to as-spun and other annealed films. Particularly, the 250 and 300 °C-annealed films showed severe degradation in μ_{FET} and hysteresis, with a negative threshold voltage (V_{th}) shift (Figure 7a). These results were related to the laterally disconnected conducting pathways (Figure 3c,d).

In contrast, TIPSBDT-DPP5OP copolymer films showed drastically enhancement in μ_{FET} values up to $1.2 \text{ cm}^2 \text{ V}^{-1} \text{ s}^{-1}$ after annealing, which induced better conjugation and ordering conducting domains (Figure 7b,c). In OFETs, the as-spun film yielded an average μ_{FET} value of $0.03 \text{ cm}^2 \text{ V}^{-1} \text{ s}^{-1}$, as well as a V_{th} of -10.0 V and an $I_{\text{on}}/I_{\text{off}}$ of about 10^4 . The 250 and 300 °C-annealed films containing layered domains yielded μ_{FET} values of 1.1 – $1.2 \text{ cm}^2 \text{ V}^{-1} \text{ s}^{-1}$ in OFETs, as well as $I_{\text{on}}/I_{\text{off}}$ values greater than 10^5 and V_{th} of -10 to -11 V. Additionally, a slight V_G -sweep hysteresis in the as-spun film disappeared after annealing (Figure 7b).

For OFETs, the charge carriers were expected to effectively transfer along the π - π overlap direction between the *S*/*D* electrodes. Therefore, the charge carrier mobility is mainly determined by the π - π stacking distance and molecular packing conformation.^[40] The significantly shorter π - π stacking distance for TIPSBDT-DPP5OP creates

Table 3. Average tilting angles of the π^* orbitals and *R* values determined by the NEXAFS spectra of the TIPSBDT-DPP-based films.

| Film | TIPSBDT-DPP2OD | | TIPSBDT-DPP5OP | |
|-----------------|----------------------------|----------|----------------------|----------|
| | α_{π^*} [°] | <i>R</i> | α_{π^*} [°] | <i>R</i> |
| As-spun | 54.3 ± 1.6 (random) | 0.012 | 68.9 ± 0.3 | 0.427 |
| 250 °C-annealed | 70.7 ± 3.1 | 0.473 | 73.6 ± 0.8 | 0.517 |

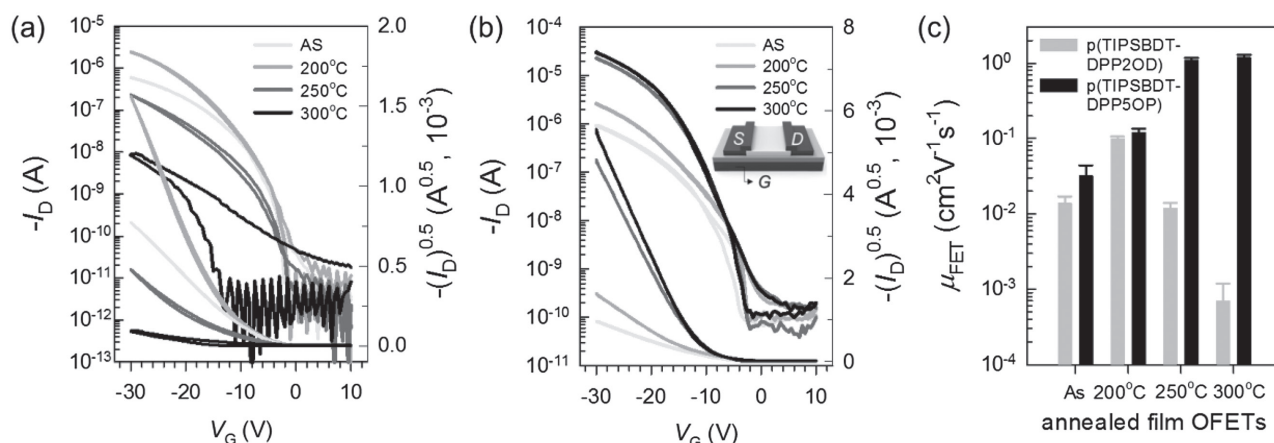


Figure 7. I_D - V_G transfer curves and the corresponding $I_D^{0.5}$ - V_G curves of OFETs including a) TIPSBDT-DPP2OD and b) TIPSBDT-DPP5OP copolymer films. c) Variations in μ_{FET} of the resulting OFETs.

TIPSBDT-DPP5OP, which had different alkyl spacers (e.g., methylene (C1) or butylene (C4)) between the DPP and $(\text{C}_{10}\text{H}_{21})\text{CH}(\text{C}_8\text{H}_{17})-$ chains, were synthesized by Suzuki cross-coupling. The longer spacer, C4, instead of C1, drastically enhanced the coplanarity and conjugation of TIPSBDT-DPP5OP in comparison to the TIPSBDT-DPP2OD copolymer. These D–A copolymer films were spun cast onto a polymer-treated SiO_2 dielectric from CB solutions and some were further annealed at 200–300 °C. By inserting the longer spacer between DPP and $(\text{C}_{10}\text{H}_{21})\text{CH}(\text{C}_8\text{H}_{17})-$, the D–A copolymer was tuned to form highly ordered and layered domains of edge-on chains, with a narrow π - π overlap spacing (up to 3.57 Å) on the dielectric surface compared to the less-conjugated short spacer system (3.93 Å). Based on the NEXAFS spectra of these films, it was found that the ordered π -conjugated planes of TIPSBDT-DPP2OD and TIPSBDT-DPP5OP were highly oriented with preferential tilting angles. For the 250 °C-annealed films, the $\alpha\pi$ values of TIPSBDT-DPP2OD and TIPSBDT-DPP5OP were 70.7° and 73.6°, respectively, with respect to the dielectric surface.

From the benefit of the side substituent creating better ordering and much closer intermolecular π -overlap, the

corresponding TIPSBDT-DPP5OP-based OFETs showed an enhancement in μ_{FET} up to $1.2 \text{ cm}^2 \text{ V}^{-1} \text{ s}^{-1}$, 12 times higher than that of the TIPSBDT-DPP2OD copolymer system. The side-chain engineering minimized the steric hindrance of the branched alkyl chains and provided new insight into the molecular design of high-performance polymer-based semiconductors.

4. Experimental Section

4.1. Materials and Sample Preparation

All solvents and reagents were purchased from Aldrich, Alfa Aesar, or TCI Korea, and some were further purified prior to use. Coupling catalysts were purchased from Strem Chemicals. Method for synthesizing DPP, benzodithiophene (BDT) derivatives, TIPSBDT-DPP2OD, and TIPSBDT-DPP5OP copolymers are depicted in Scheme 1 and the Supporting Information. The D–A copolymer was synthesized using palladium-catalyzed Suzuki coupling.^[7] The polymer was then purified using a successive soxhlet extraction with CF in order to remove excess monomers and metal catalyst residue. The final solutions were precipitated in methanol.

Thermally grown, 300 nm thick SiO_2 on a highly n-doped Si substrate was used as a primary gate dielectric. The SiO_2 surface was modified with a reactive dimethylchlorosilane-terminated polystyrene ($\text{PS-Si}(\text{CH}_3)_2\text{Cl}$, $M_n = 8000 \text{ g mol}^{-1}$; weight average molecular weight, $M_w = 8600 \text{ g mol}^{-1}$; Polymer Source Inc.). Then, 6 mg of $\text{PS-Si}(\text{CH}_3)_2\text{Cl}$ were dissolved in 1 mL of anhydrous toluene, and thin films were spun cast onto UVO_3 -treated SiO_2/Si substrates from the solution in an N_2 -purged glove box.^[8] Next, the polymer-coated SiO_2 samples were thermally treated at 110 °C for 2 h, followed by rinsing with an excess volume of toluene to remove the ungrafted polymer residue. Approximately

Table 4. Electrical properties of TIPSBDT-DPP-based copolymer OFETs, before and after annealing at different T_A .

| OFET | Film | $\mu_{\text{FET}} [\text{cm}^2 \text{ V}^{-1} \text{ s}^{-1}]$ | $V_{\text{th}} [\text{V}]$ | $I_{\text{on}}/I_{\text{off}}$ |
|----------------|-----------------|--|----------------------------|--------------------------------|
| TIPSBDT-DPP2OD | As-spun | 0.014 ± 0.003 | -8 | $>10^4$ |
| | 200 °C-annealed | 0.10 ± 0.006 | -12 | $>10^5$ |
| | 250 °C-annealed | 0.012 ± 0.002 | -14 | $>10^4$ |
| | 300 °C-annealed | <0.001 | -17 | $\approx 10^2$ |
| TIPSBDT-DPP5OP | As-spun | 0.03 ± 0.012 | -10 | $\approx 10^4$ |
| | 200 °C-annealed | 0.12 ± 0.015 | -12 | $>10^4$ |
| | 250 °C-annealed | 1.10 ± 0.08 | -10 | $>10^5$ |
| | 300 °C-annealed | 1.20 ± 0.10 | -11 | $>10^5$ |

20–25 nm thick films of TIPSBDT-DPP-based copolymers were spun cast onto the gPS-SiO₂ from 3 mg mL⁻¹ solutions prepared with CB. Some were further annealed at a temperature ranging from 200 to 300 °C for either 30 or 10 min, based on the thermal behaviors of the copolymers determined using TGA and DSC. Finally, 80 nm thick Au S/D electrodes were thermally evaporated on these D–A copolymer films through a shadow mask; the channel length (*L*) and width (*W*) were 100 and 1500 μm, respectively.

4.2. Characterization

The molecular weights (*M_n* and *M_w*) and chemical compositions of these copolymers were determined by GPC (calibrated with PS standards, Waters, M590) in 1,2-dichlorobenzene (*o*-DCB, 100 °C) and ¹H NMR (Varian Mercury Plus 300 MHz spectrometer) analyses, respectively. The thermal stability of the copolymer was measured by thermogravimetric analysis (TGA) (Mettler Toledo, TGA/SDTA 851), which was operated under an N₂ atmosphere. Additionally, DSC (TA Instrument, Q20) was performed on the powder-like polymers with a scan rate of 10 °C min⁻¹. UV–vis absorption spectra of the copolymers were measured in a dilute CB solution and in spun-cast films before and after annealing at various values of *T_A*s using a UV–vis spectrometer (JASCO JP/V-570). CV for the copolymers was performed using an electrochemical analyzer (CH Instruments, Electrochemical Analyzer) within a 0.1 M solution of TBABF₄ in acetonitrile. A glassy carbon disk (≈0.05 cm²) coated with a thin polymer film, an Ag/AgNO₃ electrode, and a platinum wire were used as the working, reference, and counter electrodes, respectively.^[7]

All the morphologies of these copolymer films on the gPS-SiO₂ surfaces were observed by AFM (Bruker, Multimode 8). The current–voltage (*I*–*V*) measurement of the OFETs was conducted in an N₂-purged glove box at room temperature, using a Keithley 4200 SCS. The values of μ_{FET} were calculated from the *I_D*–*V_G* transfer curves of the OFETs operated under the saturation region (*V_D* = –30 V) and the equation: $I_D = \mu_{FET} C_i W (2L)^{-1} (V_G - V_{th})^2$, where *C_i* is the capacitance per unit area of the dielectric. The *C_i* value (≈10.8 nF cm⁻²) for the gPS-SiO₂ dielectric, sandwiched between Au dots and a highly doped n-type Si (100) substrate, was measured with an Agilent 4284A Precision LCR meter. 2D GIXD was performed on all the films at beamlines 6D and 9A of the Pohang Acceleration Laboratory (PAL), Korea. NEXAFS was performed with a PEY detection mode at the 4D beamline of PAL. NEXAFS spectra of the D–A copolymer films were acquired by recording the sample current normalized to a signal current in ultrahigh vacuum (<10⁻⁹ Torr); the p-polarized (≈85%) photon beam, which has an energy in the range of 279–320 eV and a spectral energy resolution of Δ*E* = 0.15 eV, could probe up to ≈6 nm from a film surface.

Supporting Information

Supporting Information is available from the Wiley Online Library or from the author.

Acknowledgements: This work was supported by grants from the Center for Advanced Soft Electronics under the Global

Frontier Research Program (2012M3A6A5055225), the Industrial Fundamental Technology Development Program (10051440) funded by the Ministry of Trade, Industry and Energy (MOTIE), and National Research Foundation (NRF) grant (2011-0030013) funded by the Korea government through Global Core Research Center for Ships and Offshore Plants (GCRC-SOP), Korea.

Conflict of Interest: The authors declare no conflict of interest.

Received: March 14, 2017; Revised: April 20, 2017;
Published online: May 23, 2017; DOI: 10.1002/macp.201700135

Keywords: alkyl spacer; benzodithiophene; diketopyrrolopyrrole; organic field effect transistor; side chain engineering

- [1] J. Y. Oh, S. Rondeau-Gagné, Y.-C. Chiu, A. Chortos, F. Lissel, G.-J. N. Wang, B. C. Schroeder, T. Kurosawa, J. Lopez, T. Katsumata, J. Xu, C. Zhu, X. Gu, W.-G. Bae, Y. Kim, L. Jin, J. W. Chung, J. B.-H. Tok, Z. Bao, *Nature* **2016**, *539*, 411.
- [2] B. Kang, B. Moon, H. H. Choi, E. Song, K. Cho, *Adv. Electron. Mater.* **2016**, *2*, 1500380.
- [3] M. Jang, S. H. Kim, H.-K. Lee, Y.-H. Kim, H. Yang, *Adv. Funct. Mater.* **2015**, *25*, 3833.
- [4] M. Lee, H. Jeon, M. Jang, H. Yang, *ACS Appl. Mater. Interfaces* **2016**, *8*, 4819.
- [5] H. Yang, T. J. Shin, L. Yang, K. Cho, C. Y. Ryu, Z. Bao, *Adv. Funct. Mater.* **2005**, *15*, 671.
- [6] Y. Yuan, G. Giri, A. L. Ayzner, A. P. Zoombelt, S. C. B. Mannsfeld, J. Chen, D. Nordlund, M. F. Toney, J. Huang, Z. Bao, *Nat. Commun.* **2014**, *5*, 3005.
- [7] J.-H. Kim, M. Lee, H. Yang, D.-H. Hwang, *J. Mater. Chem. A* **2014**, *2*, 6348.
- [8] M. Pei, J. Huang, M. Jang, J.-H. Kim, M. Lee, J. Chen, D.-H. Hwang, H. Yang, *J. Phys. Chem. C* **2016**, *120*, 903.
- [9] C. B. Nielsen, M. Turbiez, I. McCulloch, *Adv. Mater.* **2013**, *25*, 1859.
- [10] Y. Li, S. P. Singh, P. Sonar, *Adv. Mater.* **2010**, *22*, 4862.
- [11] I. Meager, R. S. Ashraf, S. Rossbauer, H. Bronstein, J. E. Donaghey, J. Marshall, B. C. Schroeder, M. Heeney, T. D. Anthopoulos, I. McCulloch, *Macromolecules* **2013**, *46*, 5961.
- [12] Z. Li, Y. Zhang, S. W. Tsang, X. Du, J. Zhou, Y. Tao, J. Ding, *J. Phys. Chem. C* **2011**, *115*, 18002.
- [13] F. Zhang, Y. Hu, T. Schuettfort, C. Di, X. Gao, C. R. McNeill, L. Thomsen, S. C. B. Mannsfeld, W. Yuan, H. Siringhaus, D. Zhu, *J. Am. Chem. Soc.* **2013**, *135*, 2338.
- [14] I. Meager, R. S. Ashraf, S. Mollinger, B. C. Schroeder, H. Bronstein, D. Beatrup, M. S. Vezie, T. Kirchartz, A. Salleo, J. Nelson, I. McCulloch, *J. Am. Chem. Soc.* **2013**, *135*, 11537.
- [15] B. C. Schroeder, Y.-C. Chiu, X. Gu, Y. Zhou, J. Xu, J. Lopez, C. Lu, M. F. Toney, Z. Bao, *Adv. Electron. Mater.* **2016**, *2*, 1600104.
- [16] A.-R. Han, G. K. Dutta, J. Lee, H. R. Lee, S. M. Lee, H. Ahn, T. J. Shin, J. H. Oh, C. Yang, *Adv. Funct. Mater.* **2015**, *25*, 247.
- [17] J. H. Dou, Y. Q. Zheng, T. Lei, S. D. Zhang, Z. Wang, W. B. Zhang, J. Y. Wang, J. Pei, *Adv. Funct. Mater.* **2014**, *24*, 6270.
- [18] M. Jung, Y. Yoon, J. H. Park, W. Cha, A. Kim, J. Kang, S. Gautam, D. Seo, J. H. Cho, H. Kim, J. Y. Choi, K. H. Chae, K. Kwak, H. J. Son, M. J. Ko, H. Kim, D. K. Lee, J. Y. Kim, D. H. Choi, B. Kim, *ACS Nano* **2014**, *8*, 5988.

- [19] J. Y. Back, H. Yu, I. Song, I. Kang, H. Ahn, T. J. Shin, S.-K. Kwon, J. H. Oh, Y.-H. Kim, *Chem. Mater.* **2015**, *27*, 1732.
- [20] H. Yu, K. H. Park, I. Song, M.-J. Kim, Y.-H. Kim, J. H. Oh, *J. Mater. Chem. C* **2015**, *3*, 11697.
- [21] D. H. Kim, Y. D. Park, Y. Jang, H. Yang, Y. H. Kim, J. I. Han, D. G. Moon, S. Park, T. Chang, C. Chang, M. Joo, C. Y. Ryu, K. Cho, *Adv. Funct. Mater.* **2005**, *15*, 77.
- [22] I. McCulloch, M. Heeney, C. Bailey, K. Genevicius, I. MacDonald, M. Shkunov, D. Sparrowe, S. Tierney, R. Wagner, W. Zhang, M. L. Chabinyc, R. J. Kline, M. D. McGehee, M. F. Toney, *Nat. Mater.* **2006**, *5*, 328.
- [23] M. Jang, J.-H. Kim, D.-H. Hwang, H. Yang, *ACS Appl. Mater. Interfaces* **2015**, *7*, 12781.
- [24] J. Y. Kim, D. S. Yang, J. Shin, D. Bilby, K. Chung, H. A. Um, J. Chun, S. Pyo, M. J. Cho, J. Kim, D. H. Choi, *ACS Appl. Mater. Interfaces* **2015**, *7*, 13431.
- [25] G.-Y. Lee, A.-R. Han, T. Kim, H. R. Lee, J. H. Oh, T. Park, *ACS Appl. Mater. Interfaces* **2016**, *8*, 12307.
- [26] H. A. Um, D. H. Lee, D. U. Heo, D. S. Yang, J. Shin, H. Baik, M. J. Cho, D. H. Choi, *ACS Nano* **2015**, *9*, 5264.
- [27] D. Yoo, B. Nketia-Yawson, S.-J. Kang, H. Ahn, T. J. Shin, Y.-Y. Noh, C. Yang, *Adv. Funct. Mater.* **2015**, *25*, 586.
- [28] D. Khim, Y. R. Cheon, Y. Xu, W.-T. Park, S.-K. Kwon, Y.-Y. Noh, Y.-H. Kim, *Chem. Mater.* **2016**, *28*, 2287.
- [29] J. Cho, S. B. Lee, H.-K. Lee, S.-K. Kwon, Y.-H. Kim, D. S. Chung, *Adv. Electron. Mater.* **2016**, *2*, 1600015.
- [30] J. Yao, C. Yu, Z. Liu, H. Luo, Y. Yang, G. Zhang, D. Zhang, *J. Am. Chem. Soc.* **2016**, *138*, 173.
- [31] Y. Zhao, X. Zhao, Y. Zang, C. Di, Y. Diao, J. Mei, *Macromolecules* **2015**, *48*, 2048.
- [32] M. He, W. Li, Y. Gao, H. Tian, J. Zhang, H. Tong, D. Yan, Y. Geng, F. Wang, *Macromolecules* **2016**, *49*, 825.
- [33] V. S. Nair, J. Sun, P. Qi, S. Yang, Z. Liu, D. Zhang, A. Ajayaghosh, *Macromolecules* **2016**, *49*, 6334.
- [34] Z. Mao, W. Zhang, J. Huang, K. Shi, D. Gao, Z. Chen, G. Yu, *Polym. Chem.* **2015**, *6*, 6457.
- [35] J. Stöhr, *NEXAFS Spectroscopy*, 1st ed, Springer, Berlin **1996**.
- [36] J. Rivnay, S. C. B. Mannsfeld, C. E. Miller, A. Salleo, M. F. Toney, *Chem. Rev.* **2012**, *112*, 5488.
- [37] G. Hähner, *Chem. Soc. Rev.* **2006**, *35*, 1244.
- [38] H. Ade, A. P. Hitchcock, *Polymer* **2008**, *49*, 643.
- [39] D. M. DeLongchamp, R. J. Kline, D. A. Fischer, L. J. Richter, M. F. Toney, *Adv. Mater.* **2011**, *23*, 319.
- [40] T. Lei, J.-H. Dou, J. Pei, *Adv. Mater.* **2012**, *24*, 6457.